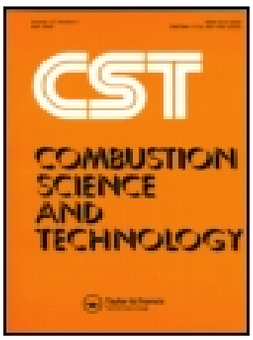

Taylor & Francis
Taylor & Francis Group

Combustion Science and Technology

ISSN: 0010-2202 (Print) 1563-521X (Online) Journal homepage: http://www.tandfonline.com/loi/gcst20

Soot Modeling of Ethylene Counterflow Diffusion Flames

Warumporn Pejpichestakul, Alessio Frassoldati, Alessandro Parente & Tiziano Faravelli

To cite this article: Warumporn Pejpichestakul, Alessio Frassoldati, Alessandro Parente & Tiziano Faravelli (2018): Soot Modeling of Ethylene Counterflow Diffusion Flames, Combustion Science and Technology, DOI: 10.1080/00102202.2018.1540472

To link to this article: https://doi.org/10.1080/00102202.2018.1540472

Published online: 31 Oct 2018.

COMBUSTION SCIENCE AND TECHNOLOGY
https://doi.org/10.1080/00102202.2018.1540472

Taylor & Francis
Taylor & Francis Group

Soot Modeling of Ethylene Counterflow Diffusion Flames

Warumporn Pejpichestakul[a,b], Alessio Frassoldati[a], Alessandro Parente [b,c], and Tiziano Faravelli [a]

[a]CRECK Modeling Lab, Department of Chemistry, Materials and Chemical Engineering "G. Natta", Politecnico di Milano, Milano, Italy; [b]Université Libre de Bruxelles, Ecole polytechnique de Bruxelles, Aero-Thermo-Mechanics Laboratory, Brussels, Belgium; [c]Combustion and Robust Optimization Group (BURN), Université Libre de Bruxelles and Vrije Universiteit Brussel, Brussels, Belgium

ABSTRACT

Combustion-generated nanoparticles cause detrimental effects to not only health and environment but also combustion efficiency. A detailed kinetic mechanism employing a discrete sectional model is validated using experimental data obtained in laminar counterflow diffusion flames of ethylene/oxygen/nitrogen. Two configurations, named Soot formation (SF) and soot formation/oxidation (SFO) flames, are modeled using one-dimensional simulations. Radiative heat losses reduce the maximum flame temperature in the range of 20–60 K and therefore reduce soot volume fraction by ~ 10%. The model predictions accounting for the radiation effects are quite satisfactory. The model can reproduce the qualitative trends of soot volume fraction peaks that are slightly shifted toward the oxidizer zone with the increased oxygen content. In SF flames, the model predicts the maximum soot volume fraction quite well with the largest discrepancy of two folds. The particle stagnation locations can be reproduced by the model, although they are slightly shifted toward the oxidizer nozzle by ~ 0.4 mm. In SFO flames, the most considerable discrepancy is observed at the least sooting flame ($x_{F,o}$ = 0.23) in which the model over-predicts the maximum soot volume fraction by a factor of two. The effect of soot oxidation is important. The model shows that neglecting oxidation of soot significantly increases soot volume fraction in SFO flames by two folds while SF flames are only marginally affected. Also, ignoring soot oxidation leads to the presence of soot particles in the oxidizer zone where they are not observed experimentally. OH is the most effective oxidizer because the sooting zone is located inside the flame region. The effect of thermophoresis is also investigated. It strongly influences SFO flames due to the high temperature gradient. The model accounting particle diffusivities from Stokes–Cunningham correlation can better characterize the distinct particle stagnation plane of SF flames due to their low diffusion coefficients.

ARTICLE HISTORY
Received 10 September 2018
Revised 17 October 2018
Accepted 22 October 2018

KEYWORDS
Soot; kinetic modeling; counterflow diffusion flames; sectional model

Introduction

Combustion-generated nanoparticles are well-known for their adverse effects on health and environment. In practical applications, the presence of soot particles leads to the radiative heat losses and consequently lowers the combustion efficiency (Bockhorn et al., 2007). Polycyclic aromatic hydrocarbons (PAHs) are widely accepted as soot precursors, and

CONTACT Tiziano Faravelli tiziano.faravelli@polimi.it

Color versions of one or more of the figures in the article can be found online at www.tandfonline.com/gcst.

acetylene plays an essential role in the soot growth processes through the sequential HACA (hydrogen abstraction and acetylene addition) mechanism (Frenklach et al., 1985; Wang and Frenklach, 1997). In addition, condensation of PAHs and gaseous species on soot particle contributes to the soot growth. On the contrary, the oxidations of particles compete with the soot growth. The oxidation processes include the burnout at the surface of particles mainly by OH radical, and the oxidation-induced fragmentation, which is the internal burning induced by the penetration of oxygen molecules into particles (Ghiassi et al., 2016).

Particulate formation and oxidation have been extensively studied in the past two decades particularly in premixed planar laminar flames (Zhang et al., 2009). In industrial or commercial combustors, however, the soot evolution becomes extremely complex due to the interactions between chemistry and turbulence flow environment (Franzelli et al., 2017). To achieve a better understanding of soot formation in turbulent flames, laminar counterflow diffusion flame configuration is a good candidate because of its well-defined boundary conditions that can simplify as one-dimensional simulations and its relevance to flamelet model, which is often adopted to model practical industrial scale applications (Chrigui et al., 2012).

There are several attempts to understand soot evolution in counterflow diffusion flames using different modeling approaches (D'Anna, 2009; Kennedy et al., 1990; Liu et al., 2004; Mehta et al., 2009; Sirignano et al., 2015; Wang and Chung, 2016). Liu et al. (2004) studied the effects of gas and soot radiation on soot formation in counterflow ethylene flames and observed that the effect of gas radiation plays more a more important role than soot radiation. Slavinskaya et al. (2012) studied PAH formation in non-premixed flames and compared the predictions with other mechanisms. They observed differences in the predictions of PAH in orders of magnitudes. In addition, predicted PAH profiles are slightly shifted toward oxidizer nozzle. Wang and Chung (2016) studied strain rate effects on sooting flames and observed that its importance is more pronounced in larger PAHs.

In this work, detailed kinetic modeling of soot formation in atmospheric laminar counterflow diffusion ethylene/oxygen/nitrogen flames has been performed and compared with the experimental studies by Hwang and Chung (Hwang and Chung, 2001). The validation includes soot formation (SF) and soot formation/oxidation (SFO) flames. The inlet velocities of fuel and oxidizer nozzles are identical at 19.5 cm/s. For SF flames, the fuel inlet was pure ethylene while the oxygen mole fraction of the oxidizer inlet (xO,o) was varied from 0.2 to 0.28. For SFO flames, the oxidizer inlet is 90% oxygen in nitrogen while the mole fraction of oxygen in the fuel inlet (xF,o) was varied from 0.23 to 0.28.

Model description and numerical simulations

The high temperature gas-phase mechanism consists of ~ 300 species and over 8000 reactions. It implements a C_0-C_3 core mechanism obtained from the H_2/O_2 and C_1/C_2 subsets from Metcalfe et al. (Metcalfe et al., 2013), C_3 from Burke et al. (Burke et al., 2015), and heavier fuels from Ranzi et al. (Ranzi et al., 2012). The model describes the pyrolysis and oxidation of wide range hydrocarbon fuels and includes the formation of PAHs up to pyrene. The thermochemical properties were obtained from the ATcT database of Rusic (Ruscic, 2015) or Burcat's database (Goos et al., 2016). For some species that were not available in the aforementioned databases, the thermochemical properties were adopted from group additivity method (Benson et al., 1969).

A soot model based on a discrete sectional approach is coupled to the gas-phase mechanism to model the evolution from gas-phase to solid particles. The model includes the discretization large PAH and soot particles into 25 sections, considered as lumped-pseudo species called "BINs", with a constant discretization spacing factor of two in terms of carbon atoms. Three hydrogenation levels are considered for each BIN as sub-sections, labeled "A", "B" and "C", which varies from 0.8 for BIN1A to 0.05 for BIN25C. The first BIN (BIN1) comprises of 20 carbon atoms. The first four BINs, BIN1-4, are considered as heavy gas PAHs. BIN5-12 are assumed as spherical soot particles. Therefore, BIN12 represents primary particle with a diameter of ~ 10 nm. On turn, soot aggregates are particles larger than the primary particle, BIN13-25, with a fractal structure, whose fractal dimension is 1.8. The inception of particles comes from reactions involving heavy PAHs. These reactions account for sticking probability, whose value depends on the size of colliding entities and the temperature, as estimated from the comparison with molecular dynamics simulations. The coagulation and aggregation of particles occur through reactions involving soot particles and aggregates. The reference rate of inception and coagulation rate is $1.6 \times 10^{13} T^n nC^{1/6}$ $\mathrm{cm^3 mol^{-1} s^{-1}}$, where the collision frequency is evaluated using the number of carbon atom, nC (Pejpichestakul et al., 2018). Other reactions (which include surface growth by acetylene addition, gaseous species and PAH condensation, dehydrogenation, H-Abstraction and oxidation), are discussed elsewhere (Saggese et al., 2015).

The complete soot mechanism used in this work (CRECK1800s) has been extensively validated against laminar premixed flames of different fuels in wide range operating conditions which is discussed elsewhere (Pejpichestakul and Ranzi et al., 2018). The successive kinetic mechanism consists of approximately 400 species and 25,000 reactions. Further details of the soot kinetics model are available in (Pejpichestakul et al., 2018; Saggese et al., 2015).

All numerical simulations were performed using OpenSMOKE++ suite program by Cuoci et al. (Cuoci et al., 2015). Laminar counterflow diffusion flames 1-D simulations were performed using the mixture-average diffusion coefficient and including thermal diffusion (Soret effect) in species transport equations for the gaseous species. Diffusivities of soot particles are obtained from Stokes Law with Cunningham correction based on Knudsen number (Friedlander, 1977). The thermophoretic flux of solid particles is also included in the model, as described in paragraph 3.3. Solution gradient and curvature coefficients of 0.05 and 0.5 were assigned to ensure the smoothness of the calculated profiles.

Radiative heat losses account for gas and soot radiation (Equation 1) using an optically thin approximation. Radiation from gaseous species is included for only significant radiating species, H_2O, CO, CO_2 and CH_4.

$$Q_{rad} = -4\sigma a_p (T^4 - T_{env}^4) \tag{1}$$

where σ is the Stefan–Boltzman constant. T_{env} is the environment temperature, for which a value of 298 K is assumed in this work. a_p is the Planck mean absorption coefficient, which can be evaluated by the following equation:

$$a_p = p_{H_2O} a_{p,H_2O} + p_{CO} a_{p,CO} + p_{CO_2} a_{p,CO_2} + p_{CH_4} a_{p,CH_4} + \kappa_{particle} \tag{2}$$

where p_i is the partial pressure of species i. $a_{p,i}$ is the extinction coefficient of species i obtained from calculations performed by the RADCAL software (Barlow et al., 2001; Grosshandler,

1993). $\kappa_{particle}$ is the grey soot absorption coefficient (Barlow et al., 2000), which is proportional to soot volume fraction (f_v):

$$\kappa_{particle} = 1307 f_v T \tag{3}$$

Results and discussions

Flame structure and effect of radiative heat losses

Figure 1 shows the effects of radiative heat losses on the predicted flame temperatures. The yellow shaded areas represent the sooting region of the two flames. The dashed lines represent the predicted temperature profiles neglecting radiation heat losses from gaseous species and soot particles. The reduction in temperature due to the heat losses increases with the flame temperature, which also represents soot propensity. SF flames have a reduction in the range of ~ 20–30 K, which agrees with the observation of Liu et al. (2004) who noticed that the effect of radiative heat losses is insignificant in these flames. The reduction of flame temperature in SFO flames is slightly higher than SF flames (~ 50–60 K) because of the higher flame temperature. As expected, the radiative heat losses reduce the maximum temperature of all flames in the range of 20–60 K.

Figure 2 shows the comparison of the soot volume fractions profiles between experimental data and model predictions. The model predictions are obtained both including and the neglecting radiative heat losses. The lower temperature reduces soot formation in all flames by approximately 10%. However, the model predictions including radiative heat losses still provide good agreement with the experimental data. It can reproduce the qualitative trends of soot volume fraction peaks that are slightly shifted toward oxidizer zone with the increased oxygen content. The model predicts the maximum soot volume fraction quite well with a slight over-prediction at the least sooting condition (xO, o = 0.20) and an under-prediction at the most sooting conditions (xO,o = 0.28). These discrepancies are within a factor of 2. The distinct particle stagnation locations can be reproduced by the model, although they are slightly shifted toward the oxidizer nozzle by ~ 0.4 mm. This result is associated with the diffusion velocity of particles which are evaluated in the model accounting for both mass (fickian) and thermophoretic diffusions.

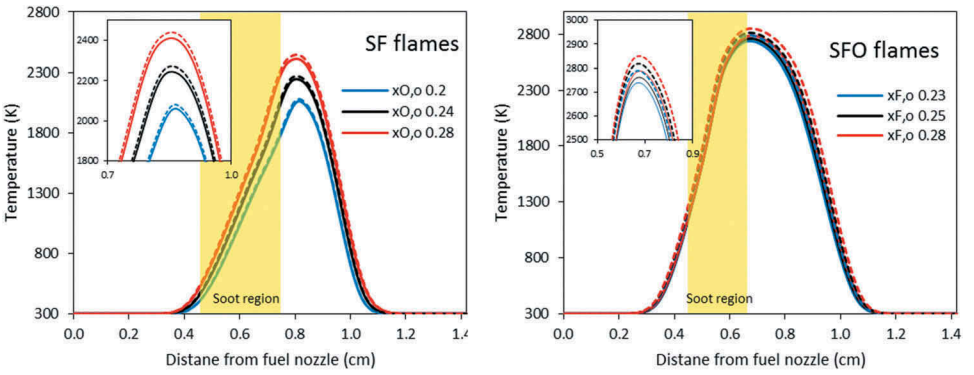

Figure 1. Calculated temperature profiles of SF flames (left panel) and SFO flames (right panel). Dashed lines: model neglecting radiative heat losses. Solid lines: model including radiative heat losses.

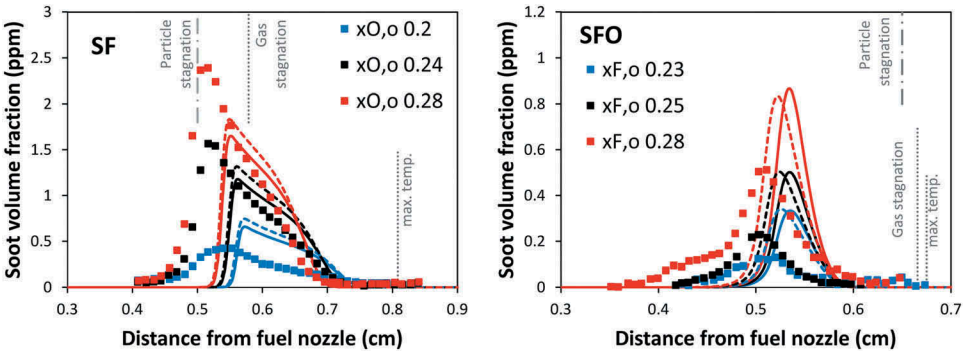

Figure 2. Comparison of soot volume fraction profiles between experimental data (symbol) and model (lines) of SF flames (left panel) and SFO flames (right panel). Dashed lines: model neglecting radiative heat losses. Solid lines: model including radiative heat losses.

Specifically for SF flames, thermophoretic diffusion enhances their movement towards the particle stagnation plane but it is much lower than the convective velocity. This suggests that the transport properties of soot particles require further attention. The most considerable discrepancy in SFO flames is observed at the least sooting flame (xF,o = 0.23), in which the model over-predicts the maximum soot volume fraction by a factor of two.

Effect of soot oxidation

To highlight the effect of soot oxidation, Figure 3 shows the effect of soot oxidation on the predicted soot volume fraction in comparison with the measurements. As expected, in SF flames, soot oxidation has marginal effects, since soot particles are pushed away from the sooting region of the flames and are convected toward the fuel inlet. On the contrary, in SFO flames, the removal of particle oxidation increases soot volume fraction drastically by as high as approximately 50%. Additionally, the soot particles are able to form and diffuse toward the oxidizing zone where soot particles are not observed

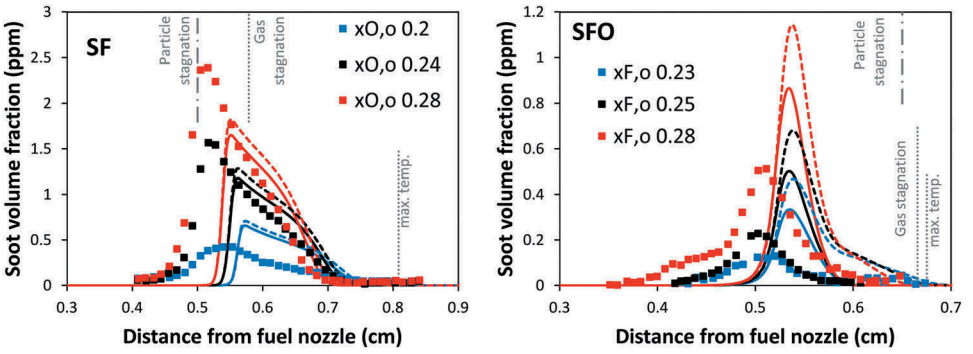

Figure 3. Comparison of soot volume fraction profiles between experimental data (symbol) and model (lines) of SF flames (left panel) and SFO flames (right panel). Dashed lines: model neglecting soot oxidation. Solid lines: model including soot oxidation.

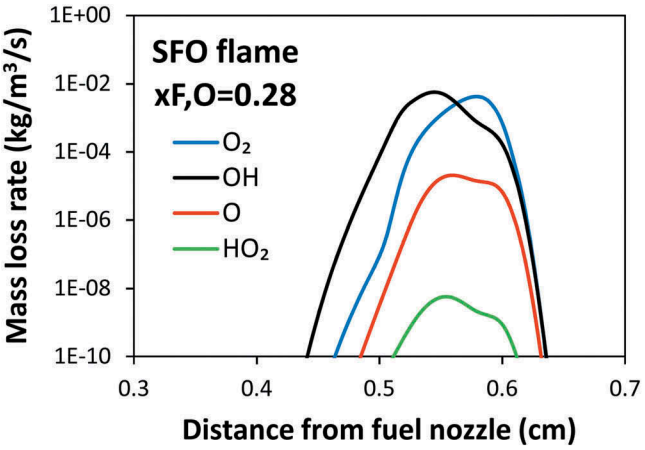

Figure 4. Mass loss rate of particle oxidation by different oxidizers.

experimentally. The successful predictions using the complete soot model in SFO flames demonstrate that the reaction rates of the processes involved in soot growth and oxidation are appropriate.

To better understand the particle oxidation, Figure 4 shows the mass loss rate by different oxidizers along the distance from fuel nozzle of xF,o = 0.28 flame. Soot particles form and are transported within the high temperature flame zone. Therefore, soot particles are oxidized mainly by OH radical, whereas O_2 plays an important role only close to the oxidizer nozzle.

Effect of thermophoresis

The temperature along the axial coordinate is ranging from 300 to over 2000 K as highlighted in Figure 1. Sooting zones of all flames fall within this high temperature zone, which is characterized by large temperature gradients. Therefore, the thermophoretic effect is investigated in this paragraph. Figure 5 shows the effect of thermophoresis in

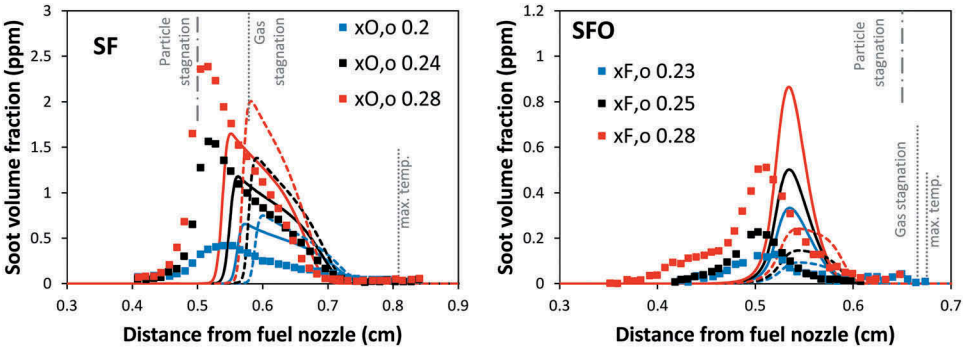

Figure 5. Comparison of soot volume fraction profiles between experimental data (symbol) and model (lines) of SF flames (left panel) and SFO flames (right panel). Dashed lines: model neglecting thermophoretic effect. Solid lines: model including thermophoretic effect.

comparison with experimental data. Unsurprisingly, thermophoretic force pushes solid particles away from high temperature toward the colder side, which is the region close to the fuel nozzle. In SF flames, thermophoretic velocity shifts soot volume fraction profiles by ~ 0.2 mm toward gas stagnation plane, resulting in a lower peak of volume fraction of soot particles. Thermophoretic flux plays a more important role in SFO flame due to the higher temperature gradient in comparison to SF flames. Thermophoresis pushes soot particles away from the gas stagnation plane, which competes with the convection/diffusion toward gas stagnation. Consequently, it increases soot volume fractions in SFO flames. This results agrees with the findings by Gomez and Rosner (1993) that thermophoresis can influence particle flow history in non-premixed flame. This suggests that the transport properties of soot particles should be investigated further, in particular thermophoresis, which plays a major role in these conditions (Stagni et al., 2018).

Effect of particle diffusivity

It is important to examine the effect of mass diffusion or particle diffusivity to understand sooting characteristics. Figure 6 compares the diffusion coefficient of lumped pseudo species obtained from gas kinetic theory and Stokes–Cunningham correlation. The dashed line shows the mutual diffusion coefficient obtained from gas kinetic theory from Hirschfelder et al. (Hirschfelder et al., 1954) by using the transport properties from (Richter et al., 2005). Transport properties of particles larger than BIN4 (~ 2 nm) are kept constant. This assumption results in high diffusion coefficients since it is treated as a gaseous species. On the contrary, the diffusion coefficients obtained from Stokes–Cunningham decrease with the increase of molecular weight or particle size. The values obtained from these two different approaches are then applied to demonstrate the effect of mass diffusion.

Figure 7 shows the comparison of soot volume fraction profiles between measurements and model predictions using different particle diffusivities. The model with lower diffusion coefficients deriving from Stokes-Cunningham correlation provides the distinct particle stagnation as observed experimentally in SF flames at heavier sooting conditions. On the

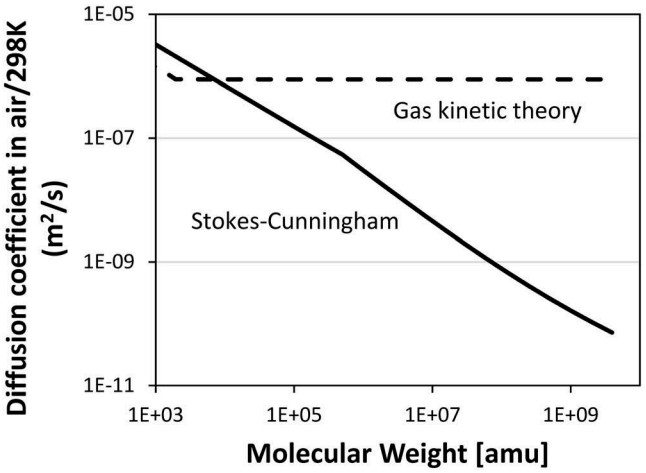

Figure 6. Diffusion coefficient of lumped pseudo species respect to molecular weight.

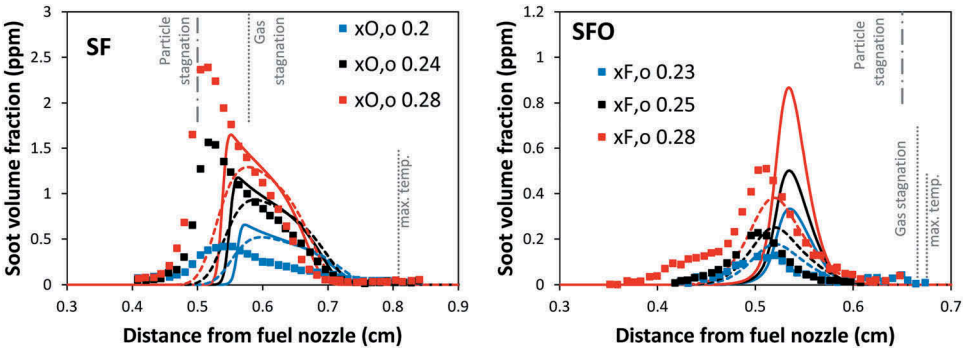

Figure 7. Comparison of soot volume fraction profiles between experimental data (symbol) and model (lines) of SF flames (left panel) and SFO flames (right panel). Dashed lines: model accounting particle diffusivity from gas kinetic theory. Solid lines: model accounting particle diffusivity from Stoke-Cunningham correlation.

contrary, in the lower sooting case (xO,o = 0.2), the measurement did not show a distinct particle stagnation plane as predicted by the model. This could be either the result of the slightly too low particle diffusivities, which also reduce thermal diffusion flux from Soret effect. In SFO flames, surprisingly, the model with diffusion coefficients deriving from gas kinetic theory, which has higher diffusivities, provides better agreement with the measurements. The higher diffusivities increase thermal diffusion from Soret effect, which pushes particles closer to the fuel nozzle and lowers soot formation.

Conclusions

This work contains the validation of a detailed kinetic mechanism employing a discrete sectional soot model using experimental results from two different laminar counterflow diffusion ethylene flames configurations. Soot formation (SF) and soot formation/oxidation (SFO) flames at different oxygen content have been analyzed. All numerical simulations are performed using one-dimensional simulations considering radiative heat losses.

The inclusion of radiative heat losses lowers the maximum temperature by 20–60 K. The reduction of temperature leads to a lower soot volume fractions in all flames by 10%. Model predictions accounting for radiative heat losses provide good agreement with the experimental data. In SFO flames, the difference of maximum soot volume fraction between the experiment and model is approximately a factor of two. In SF flames, the largest discrepancy in soot formation is observed at the most sooting flame conditions (xO,o = 0.28), in which the model under-predicts the soot volume fraction by a factor of two. The model can successfully reproduce the distinct particle stagnation with only ~ 0.4 mm shifted toward oxidizer nozzle. These discrepancies show that the convection and diffusion of particles away from the flame is insufficient. This result is associated with the thermophoresis diffusion velocity of particles which enhances their movement toward the particle stagnation plane. This suggests that transport properties and particularly thermophoresis of soot particles may require further attention.

The effect of soot oxidation is also investigated. The model shows that neglecting oxidation, the total soot volume fraction increases significantly in SFO flames by ~ 50%.

On the contrary, SF flames are only slightly affected by soot oxidation. In addition, the absence of soot oxidation leads to the presence of soot particles in the oxidizer zone of SFO flames, where they are not observed experimentally.

Thermal and mass diffusions of soot particles are analyzed. Thermophoretic effect plays an important role particularly in SFO flames, which have high temperature gradients. In SFO flames, thermophoretic force drives soot particles toward the fuel nozzle, which increases soot formation as it competes with the convection/diffusion away from the gas stagnation plane. On the contrary, soot volume fraction profiles slightly decrease in SF flames because of the push of thermophoretic flux on soot particles toward the gas stagnation plane. The effect of mass diffusion plays a significant role in controlling the particle stagnation plane in SF flames. The mutual diffusion coefficient calculated from two different approaches (gas kinetic theory and Stokes–Cunningham correlation) are compared. The distinct particle stagnation of SF flames can be reproduced with lower particle diffusivities from the Stokes–Cunningham equation approach.

Funding

This project has received funding from the European Union's Horizon 2020 research and innovation programme under the Marie Sklodowska-Curie grant agreement No 643134.

ORCID

Alessandro Parente http://orcid.org/0000-0002-7260-7026
Tiziano Faravelli http://orcid.org/0000-0001-8382-7342

References

Barlow, R.S., *et al.* 2000. *Computational fluid dynamics in industrial combustion*, 1st edn. Edited by R. S. Barlow et al, CRC Press, New York. Available at: https://www.crcpress.com/Computational-Fluid-Dynamics-in-Industrial-Combustion/Jr-Gershtein-Li/p/book/9780849320002.

Barlow, R.S., Karpetis, A.N., Frank, J.H., and Chen, J.-Y. 2001. Scalar profiles and NO formation in laminar opposed-flow partially premixed methane/air flames. *Combust. Flame*, **127**(3), 2102–2118. doi:10.1016/S0010-2180(01)00313-3.

Benson, S.W., *et al.* 1969. Additivity rules for the estimation of thermochemical properties. *Chem. Rev.* doi:10.1021/cr60259a002.

Bockhorn, H., D'Anna, A., Sarofim, A.F., and Wang, H. Combustion generated fine carbonaceous particles 2007. doi: 10.5445/KSP/1000013744.

Burke, S.M., Burke, U., Mc Donagh, R., Mathieu, O., Osorio, I., Keesee, C., Morones, A., Petersen, E.L., Wang, W., DeVerter, T.A., Oehlschlaeger, M.A., Rhodes, B., Hanson, R.K., Davidson, D.F., Weber, B. W., Sung, C.-J., Santner, J., Ju, Y., Haas, F.M., Dryer, F.L., Volkov, E.N., Nilsson, E.J.K., Konnov, A.A., Alrefae, M., Khaled, F., Farooq, A., Dirrenberger, P., Glaude, P.-A., Battin-Leclerc, F., and Curran, H.J. 2015. An experimental and modeling study of propene oxidation. Part 2: ignition delay time and flame speed measurements. *Combust. Flame*, **162**(2), 296–314. doi:10.1016/j.combustflame.2014.07.032.

Chrigui, M., *et al.* 2012. Partially premixed reacting acetone spray using LES and FGM tabulated chemistry. *Combust flame. Elsevier*, **159**(8), 2718–2741. doi:10.1016/J.COMBUSTFLAME.2012.03.009.

Cuoci, A., *et al.* 2015. Open SMOKE++: an object-oriented framework for the numerical modeling of reactive systems with detailed kinetic mechanisms. *Comput. Phys. Commun*, **192**, 237–264. doi:10.1016/j.cpc.2015.02.014.

D'Anna, A. 2009. Combustion-formed nanoparticles. *Proc. Combustion Inst.*, **32**(1), 593–613. doi:10.1016/j.proci.2008.09.005.

Franzelli, B., *et al.* 2017. Numerical investigation of soot-flame-vortex interaction. *Proc. Combustion Inst.*, **36**(1), 753–761. Elsevier Inc.. doi:10.1016/j.proci.2016.07.128.

Frenklach, M., *et al.* 1985. Detailed kinetic modeling of soot formation in shock-tube pyrolysis of acetylene. *Symp. Int. Combust. Proc.*, **20**(1), 887–901. doi:10.1016/S0082-0784(85)80578-6.

Friedlander, S.K. 1977. *Smoke, Dust, and Haze: Fundamentals of Aerosal Behavior*, John Wiley & Sons, New York.

Ghiassi, H., Toth, P., Jaramillo, I.C., and Lighty, J.S. 2016. Soot oxidation-induced fragmentation: part 1: the relationship between soot nanostructure and oxidation-induced fragmentation. *Combust. Flame*, **163**, 179–187. doi:10.1016/j.combustflame.2015.09.023.

Gomez, A., and Rosner, D.E. 1993. Thermophoretic effects on particles in counterflow laminar diffusion flames. *Combustion Sci. Technol*, **89**(5–6), 335–362. doi:10.1080/00102209308924118.

Goos, E., Burcat, A., and Ruscic, B. 2016. *BurcatThermo*. Available at: http://garfield.chem.elte.hu/Burcat/burcat.html (Accessed: 1 May 2017).

Grosshandler, W. 1993. RadCal: A narrow band model for radiation calculations in a combustion environment. NIST technical note TN 1402. https://nvlpubs.nist.gov/nistpubs/Legacy/TN/nbstechnicalnote1402.pdf

Hirschfelder, J.O., Curtiss, C.F., and Bird, R.B. 1954. *Molecular Theory of Gases and Liquids*, John Wiley & Sons, New York.

Hwang, J.Y., and Chung, S.H. 2001. Growth of soot particles in counterflow diffusion flames of ethylene. *Combust. Flame*, **125**(1–2), 752–762. Elsevier. doi:10.1016/S0010-2180(00)00234-0.

Kennedy, I.M., Kollmann, W., and Chen, J.-Y. 1990. A model for soot formation in a laminar diffusion flame. *Combust. Flame*, **81**(1), 73–85. doi:10.1016/0010-2180(90)90071-X.

Liu, F., Guo, H., J. Smallwood, G., and El Hafi, M. 2004. Effects of gas and soot radiation on soot formation in counterflow ethylene diffusion flames. *J. Quant. Spectrosc. Radiat. Transfer*, **84**(4), 501–511. doi:10.1016/S0022-4073(03)00267-X.

Mehta, R.S., Haworth, D.C., and Modest, M.F. 2009. An assessment of gas-phase reaction mechanisms and soot models for laminar atmospheric-pressure ethylene–air flames. *Proc. Combustion Inst.*, **32**(1), 1327–1334. doi:10.1016/j.proci.2008.06.149.

Metcalfe, W.K., *et al.* 2013. A hierarchical and comparative kinetic modeling study of C1-C2hydrocarbon and oxygenated fuels. *Int. J. Chem. Kinet.*, **45**(10), 638–675. doi:10.1002/kin.20802.

Pejpichestakul, W., Frassoldati, A., Parente, A., and Faravelli, T. 2018. Kinetic modeling of soot formation in premixed burner-stabilized stagnation ethylene flames at heavily sooting condition. *Fuel*, **234**(July), 199–206. Elsevier. doi:10.1016/j.fuel.2018.07.022.

Pejpichestakul, W., Ranzi, E., *et al.* 2018. Examination of a soot model in premixed laminar flames at fuel-rich conditions. *Proc. Combustion Inst.*, 1–9. Elsevier Inc. doi:10.1016/j.proci.2018.06.104.

Ranzi, E., Frassoldati, A., Grana, R., Cuoci, A., Faravelli, T., Kelley, A.P., and Law, C.K. 2012. Hierarchical and comparative kinetic modeling of laminar flame speeds of hydrocarbon and oxygenated fuels. *Prog. Energy Combustion Sci.*, **38**(4), 468–501. doi:10.1016/j.pecs.2012.03.004.

Richter, H., Granata, S., Green, W.H., and Howard, J.B. 2005. Detailed modeling of PAH and soot formation in a laminar premixed benzene/oxygen/argon low-pressure flame. *Proc. Combustion Inst.*, **30**(1), 1397–1405. doi:10.1016/j.proci.2004.08.088.

Ruscic, B. 2015. Active thermochemical tables: sequential bond dissociation enthalpies of methane, ethane, and methanol and the related thermochemistry. *J. Phys. Chem.*, **119**(28), 7810–7837. doi:10.1021/acs.jpca.5b01346.

Saggese, C., Ferrario, S., Camacho, J., Cuoci, A., Frassoldati, A., Ranzi, E., Wang, H., and Faravelli, T. 2015. Kinetic modeling of particle size distribution of soot in a premixed burner-stabilized stagnation ethylene flame. *Combust. Flame*, **162**(9), 3356–3369. The Combustion Institute. doi:10.1016/j.combustflame.2015.06.002.

Sirignano, M., Kent, J., and D'Anna, A. 2015. Further experimental and modelling evidences of soot fragmentation in flames. *Proc. Combustion Inst.*, **35**(2), 1779–1786. doi:10.1016/j.proci.2014.05.010.

Slavinskaya, N.A., Riedel, U., Dworkin, S.B., and Thomson, M.J. 2012. Detailed numerical modeling of PAH formation and growth in non-premixed ethylene and ethane flames. *Combust. Flame*, **159**(3), 979–995. The Combustion Institute. doi:10.1016/j.combustflame.2011.10.005.

Stagni, A., Cuoci, A., Frassoldati, A., Ranzi, E., and Faravelli, T. 2018. Numerical investigation of soot formation from microgravity droplet combustion using heterogeneous chemistry. *Combust. Flame*, **189**, 393–406. Elsevier Inc. doi: 10.1016/j.combustflame.2017.10.029.

Wang, H., and Frenklach, M. 1997. A detailed kinetic modeling study of aromatics formation, growth and oxidation in laminar premixed ethylene and acetylene flames. *Combust. Flame*, **2180** (97), 173–221. doi:10.1016/S0010-2180(97)00068-0.

Wang, Y., and Chung, S.H. 2016. Strain rate effect on sooting characteristics in laminar counterflow diffusion flames. *Combust. Flame*, **165**, 433–444. doi:10.1016/j.combustflame.2015.12.028.

Zhang, H.R., Eddings, E.G., Sarofim, A.F., and Westbrook, C.K. 2009. Fuel dependence of benzene pathways. *Proc. Combustion Inst.*, **32**(1), 377–385. The Combustion Institute. doi:10.1016/j.proci.2008.06.011.